

Autofrettage effects on strength and deformation of fiber reinforced pressure vessel

X. Wang[†] and X. Chen

Department of Engineering Mechanics, School of Naval Architecture and Civil Engineering, Shanghai Jiaotong University, Shanghai 200240, P. R. China

(Received July 3, 2006, Accepted April 25, 2007)

Abstract. Based on the composite finite element simulation and a series of hydrostatic pressure and burst tests, autofrettage effects on strength and deformation of fiber reinforced pressure vessel with metallic liners have been studied in the paper (autofrettage: during the course of one pressure taking effect, the increasing internal stress in metallic liner can surpass the yielding point and the plastic deformation will happen, which result in that when there is no internal pressure, there are press stress in liner while tensile stress in fiber lamination). By making use of a composite finite element Ansys code and a series of experiments, the autofrettage pressure is determined in order to make the aluminium liner be totally in elastic state, under given hydrostatic test pressure. The stress intensity factors of the longitudinal crack in aluminum liner end under internal pressure and thermal loads have been computed and analyzed before and after the autofrettage processing. Through numerical calculation and experiment investigations, it is found that a correct choice for autofrettage pressure can improve the gas-tightness and fatigue strength of FRP vessel.

Keywords: fiber reinforced pressure vessels; autofrettage process; thermal load; stress intensity factor.

1. Introduction

Composite material reinforced structure has many advantages such as high specific strength and specific stiffness and excellent fail-safety, as well as those material properties can be designed. The use of composite materials improves the performance of the pressure vessels and offers a significant amount of material saving (Ben *et al.* 2006, Vasiliev *et al.* 2003, Okamoto and Omura 2005, Mirza *et al.* 2001, John 2004). Authors (Ben *et al.* 2006) described that fiber reinforced pressure vessels are now widely used in compressed natural gas vehicles and have a possibility to be employed in fuel cell vehicles for highly compressed hydrogen. Composite pressure vessels made by continuous winding of fibrous tapes reinforced in longitudinal and transverse directions are investigated and proposed for commercial applications instead of traditional isotensoid vessels designed for minimum mass and made by winding of unidirectional fibrous bands in Vasiliev *et al.* (2003). Although the use of fiber reinforced composites has steadily increased over the last few decades and the use of composites allows designers to optimize material usage, the analysis becomes fairly complex (Mirza *et al.* 2001). A triaxial stress analysis method for pressure vessels composed of two

[†] Ph.D., Corresponding author. E-mail: xwang@sjtu.edu.cn

layers of orthotropic elasto-plastic materials is presented by Okamoto and Omura (2005). For the use of fiber reinforced composites vessel, the study on the structural integrity of the reactor pressure vessel under pressurized thermal shock (PTS) is very important. Author (Jhung MJ and Park YW 1999) described the stress distribution and stress intensity factors of the reactor pressure vessel with a wide range of crack sizes for given material properties and transient histories such as temperature and pressure. Authors (Yao and Xu *et al.* 2004a, Yao and Chen 2004b) presented applications of the digital speckle correlation method (DSCM) for the full-field deformation measurement of carbon fiber/epoxy composite pressure vessel and the basic principles of displacement measurement using the DSCM. Based on the optical method of caustics, the local stress singularities of laminated composite materials under concentrated loads are studied in Yao and Meng (2005). Author (Meng and Jin 2006) presented a useful method of field deformation monitoring of fiber composite pressure vessel using 3D digital speckle.

Because the fiber reinforced pressure vessel with metallic liner studied in this paper has the advantages such as high specific strength, excellent air impermeability and high specific capacity, it has been paid much attention (Xia *et al.* 2001, Wild and Vichers 1997, Levend and Nuran 2002, Antonelli and Van 2001, Liu 1997). For the fiber reinforced pressure vessel with aluminum liner, the strength, gas-tightness and the high ratio of capacity to weight are thought of as important properties of the vessel. To lengthen the lifetime of the fiber reinforced pressure vessel, the maximum stress in aluminum liner layer must be below its yield limit and the working stress of fiber-reinforced layer should be below the strength limit of the material itself. Thus, the aluminum liner of the fiber reinforced vessel can always stay at the elastic state under serving or hydrostatic pressure, which ensures that the vessel has good gas tightness and long fatigue lifetime. Because the strength of the fiber layer is far higher than the aluminum liner (the former is about ten times higher than the latter), the main concern in this paper is to obtain the best stress distribution, in which the stress in the aluminum liner is lower than the yield limit and the stress in the fiber reinforced layer is below the strength of the fiber layer without increasing the thickness of the vessel. Some works on structural design and stress analysis of fiber reinforced pressure vessel with metallic liners have been done by using netting analysis, membrane theory and plain strain laminated structural analysis in References (Xia *et al.* 2001, Wild and Vichers 1997, Levend and Nuran 2002, Antonelli and Van 2001, Liu 1997). However, in their structural analyses, autofrettage process technology was not detailly considered.

In this paper, a fiber reinforced pressure vessel with aluminium liner has been taken into account as an example, and the structure design and stress analysis have been finished by using composite finite element calculations and hydrostatic pressure experiments. T700/Epoxy is chosen as composite material reinforced lamination and T6061 aluminum is as a liner layer. The optimal ratio of capacity to weight arrives at the maximum. In order to obtain the maximum ratio of capacity to weight and decrease the stress value of liner, the determination of the autofrettage pressure is a key.

Usually a ($\pm\varphi^0$, 90^0) lamination is used in filament winding pressure vessel technology. Helical ($\pm\varphi^0$) plies form geodetic domes and the circumferential (90^0) layer is added to reinforce the cylindrical part of the vessel. Because the aluminium liner decides the outer shape of the total structure, the outer shape of liner ends play an important role in deciding the stress level in the end of the fiber reinforced lamination. On the basis of the grid theory (Tsai 1980, 1985), the zero-tension curve corresponding to optimal shape of the fiber lamination is taken. In this paper, we make the mid-surface shape of the fiber winded lamination beyond the curve of aluminium liner ends most close to zero-tension curve, in other hand, guarantee that the aluminium liner seal ends

work under low stress level.

In a really example, the stacking squence of fiber reinforced lamination is composed of helical winding and circumferential winding, which can respectively reinforce longitudinally and circumferential to optimal extend through composite finite element simulation. When the vessel is under hydrostatic pressure, the only way to distribute the stress optimally between the fiber reinforced lamination and aluminium liner is to apply autofrettage process (during the course of one pressure taking effect, the increasing internal stress can surpass the yielding point and the plastic deformation will happen, which result in that when there is no internal pressure, there are press stress in the liner while tensile stress in fiber lamination).

Through the stress analysis and strain measure before and after autofrettage, it has been demonstrated that before autofrettage, the stress value in the aluminium liner is very high and near the yield stress of the liner material when the vessel is under the pressure of 30 Mpa, and while the stress value in the aluminium liner is very low after autofrettage when the vessel is under the same pressure. So, it can be seen that autofrettage process makes the aluminum liner sustain the loads within the elastic phrase, which can heighten greatly the air impermeability and fatigue property of the vessel.

The other hand, the crackle likely appearing in the top of liner seal end of the vessel has also been analyzed numerically. The calculation has demonstrated that the autofrettage process makes the crackle in the top of liner seal end of the vessel close and decreases the stress intensity factor.

Due to the friction effect between aluminium liner and gas while the vessel is inflated, the aluminium liner will endure thermal loads. Under the thermal loading, the stress intensity factor of crackle in the top of the liner seal end will increase a little and the crackle appears in opening trendence.

2. Design of the shape of the liner seal ends

The actual model of the fiber reinforced pressure vessel with aluminium liner is shown in Fig. 1. The structure is composed of fiber reinforced layers and aluminium liner. Because the seal ends

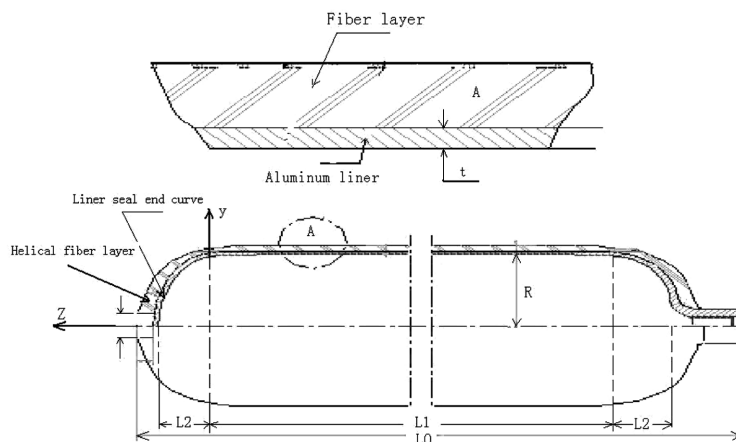


Fig. 1 The geometry structure of FRP vessel

cannot be wound circularly, the longitudinal helical winding fiber layer provides the reinforcing effect here.

The optimal seal ends of fiber layer based on the grid theory is those with zero tension curve (Tsai 1985) and the meridian equation is

$$\xi = \frac{1}{2} \int_{\lambda}^1 \frac{\sqrt{\lambda}}{\sqrt{1-\lambda^2}} d\lambda \tag{1}$$

where $\lambda = y/R$, $\xi = z/R$ and R is the radius of aluminum liner. When a seal end with such a shape received uniform internal pressure, the circular film internal force equals naught. However, the metallic liner ends of fiber reinforced pressure vessel can resist the bending and shear, so the design thought of the grid theory is not suitable for the computational model of the pressure vessel with fiber reinforced aluminium liner. Only when the load-supporting properties of the aluminium liner and composite material layer are taken synthetically into consideration and the both material exert their physical properties to the utmost extent, is such optimum shape of end. Because the aluminium liner and the fiber reinforced layer will be incorporated into one integer after being solidified and because of the thickness of fiber-reinforced layer, the optimal end shape of liner should lie in within the zero-tension curve. In the actual model, the ellipse is applied to simulate zero-tension curve. The ellipse with eccentricity of 0.56 and 0.6 are both close to and within the zero-tension curve, which is shown in Fig. 2.

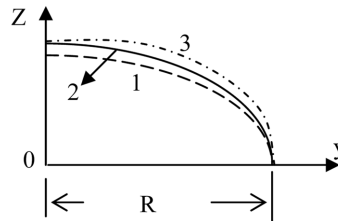


Fig. 2 The shape curves of liner seal end: 1--The ellipse with 0.56 eccentricity; 2--The ellipse with 0.6 eccentricity; 3--The zero tension curve

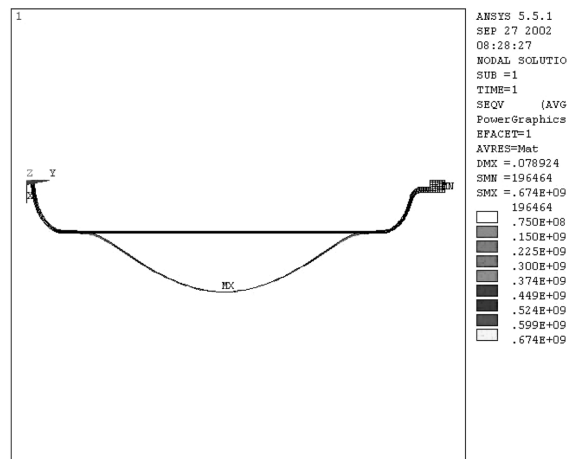


Fig. 3 The distribution of Von Miss stress (Pa) in aluminum liner under internal pressure (11 MPa), and considering non-linear effects of material and deformation

In actual structure, there exists bending effect in the linking part between the liner seal ends and cylinder and it is difficult to find theoretical solution. In this paper, the finite element Program is applied to analyze the stress distribution of the various shapes of the ends with different thickness. The finite element model of liner seal end with variable thickness is shown in Fig. 3, in which the normal space between the internal curve and the outer curve of end is the thickness of the end. Here take one point (y_0, z_0) on the outer curve and the corresponding point (y_1, z_1) on the internal curve into account, when the outer curve of the seal end is ellipse with eccentricity of 0.6, the equation of the internal and outer curve are respectively

$$\text{outer curve} \begin{cases} y_0 = 70.7 \cos \alpha \\ z_0 = 42.42 \sin \alpha \end{cases}, \quad \alpha \in [0^\circ, 90^\circ] \quad (2a)$$

$$\text{internal curve} \begin{cases} y_1 = y_0 - \sqrt{h^2 - (z_1 - z_0)^2} \\ z_1 = z_0 - h \sqrt{\frac{70.7^2 - y_0^2}{70.7^2 - 0.64y_0^2}} \end{cases} \quad (2b)$$

When the outer curve of the seal end is ellipse with eccentricity of 0.56, the equation of the internal and outer curve are respectively

$$\text{outer curve} \begin{cases} y_0 = 70.7 \cos \alpha \\ z_0 = 39.59 \sin \alpha \end{cases}, \quad \text{where } \alpha \in [0^\circ, 90^\circ] \quad (3a)$$

$$\text{internal curve} \begin{cases} y_1 = y_0 - \sqrt{h^2 - (z_1 - z_0)^2} \\ z_1 = z_0 - h \sqrt{\frac{70.7^2 - y_0^2}{70.7^2 - 0.69y_0^2}} \end{cases} \quad (3b)$$

When the outer curve of the seal end is zero-tension curve, the equation of the internal and outer curve are respectively

$$\text{outer curve} \begin{cases} y_0 = 70.7 \xi \\ z_0 = 70.7 \int_{\xi}^1 \frac{\xi^2}{\sqrt{1 - \xi^4}} d\xi \end{cases}, \quad \text{where } \xi, \lambda > 0 \quad (4a)$$

$$\text{internal curve} \begin{cases} y_1 = y_0 - \frac{hy_0^2}{70.7^2} \\ z_1 = z_0 - h \sqrt{h^2 - (y_1 - y_0)^2} \end{cases} \quad (4b)$$

From Table 1 the results of finite element calculation for three different liner ends shape can be

Table 1 The ratio of the maximum principal stress to internal pressure in the end of aluminum liner under internal pressure

The liner seal end of ellipse with eccentricity of 0.6	The liner seal end of ellipse with eccentricity of 0.56	The liner seal end with zero tension curve
2.0	2.5	2.3

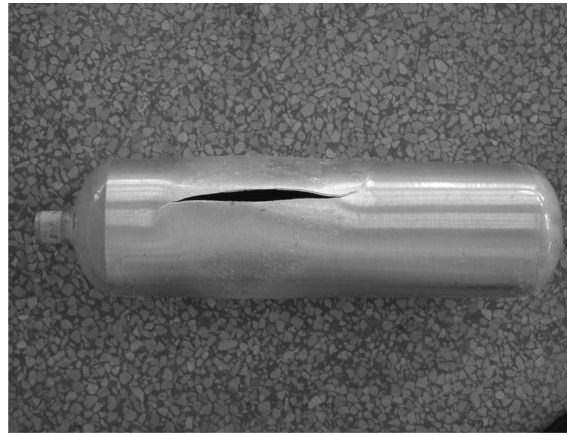


Fig. 4 The breakage form of aluminum liner under 11.4 MPa internal pressure

seen. Both the maximum Von Miss stress of the ellipse-shaped seal end with eccentricity of 0.56 and the seal end with zero tension curve is bigger than the corresponding stress of the ellipse seal end with eccentricity of 0.6. Consequently, in actual structure, it is more rational to use the ellipse-shaped aluminium liner seal end with eccentricity of 0.6, which can be expressed analytically and bring about much convenience to the design and figuration. Comparing Fig. 3 and Fig. 4 it is seen that the burst pressure (11 MPa) from the finite element simulation and really burst pressure (11.4 MPa) from the burst test is identical.

3. Finite element simulation and experiment of autofrettage

The FRP vessel is composed of aluminium liner and fiber reinforced layers. The aluminum liner is taken as isotropy hardening plastic material. The corresponding material's properties are expressed as

$$E = 69 \text{ GPa}, \quad \nu = 0.33, \quad \sigma_s = 285 \text{ MPa}, \quad \sigma_b = 310 \text{ MPa} \quad \text{and} \quad \delta \geq 14\%$$

The fiber reinforced layer is taken as T700/Epoxy with fiber volume ratio $V_f = 0.62$. By uniaxial tension tests, the material's property is taken as a linear elastic, and is given by

$$E_L = 145 \text{ GPa}, \quad E_T = E_B = 11 \text{ GPa}, \quad \nu_{LT} = \nu_{LB} = 0.3, \quad G_{LT} = 5 \text{ GPa}$$

where L , T and B express the three main directions of fiber material, respectively, and $\sigma_{Lb} = 2550 \text{ MPa}$ expresses the uniaxial tension strength in the longitudinal direction of fiber.

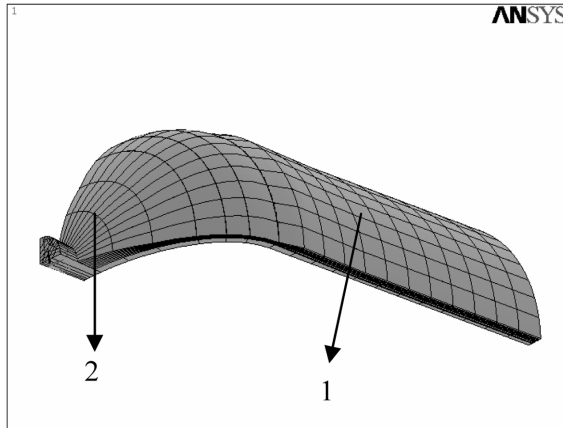


Fig. 5(a) Finite element calculation model of FRP vessel : quarter part with neck of the FRP vessel

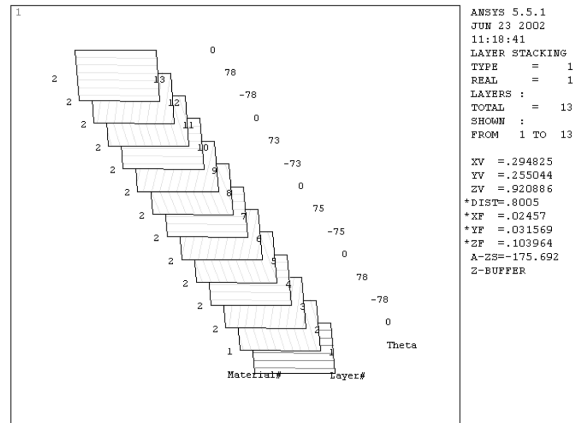


Fig. 5(b) Stacking sequence at cylindrical part (1) in the finite element calculation model (Fig. 6a)

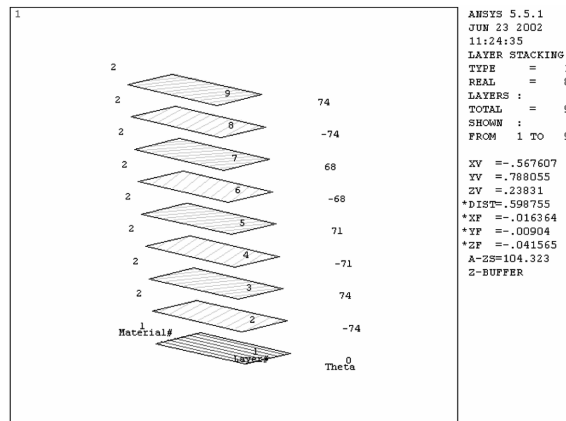


Fig. 5(c) Stacking sequence at neck end part (2) in the finite element calculation model (Fig. 6a)

Because the thicknesses of fiber layers and aluminum liner of FRP vessel gradually increase from cylinder part to seal end or neck part as shown in Fig. 1, the plastic deformation of liner and the burst of fiber layer will firstly and mainly take place in the cylinder part of the FPP vessel under internal pressure. Because of axisymmetry of FRP vessel, quarter part of the FRP vessel is taken as the computing model of composite finite element optimum design, and is shown in Fig. 5(a). A nonlinear-layered shell element, shell-91, is used in fiber-reinforced lamination and an elastoplastic element, solid95, is used in liner layer (ANSYS 1997). Stacking sequences of FRP vessel are respectively expressed as $[A/\pm 78^\circ/0^\circ/\pm 75^\circ/0^\circ/\pm 73^\circ/0^\circ/\pm 78^\circ/0^\circ]$ in the cylinder part of FRP vessel and $[A/\pm \alpha_1/\pm \alpha_2/\pm \alpha_3/\pm \alpha_1]$ in the two end parts of the FRP vessel, where the stacking angles expresses an angle between fiber longitudinal direction and the circumference of FRP vessel, which are shown in Figs. 5(b) and 5(c). Based on the finite element computing model, and according to the maximum tension failure criterion of composite laminated structures, the burst pressure from the finite element simulation is obtained as follows 110 MPa, where the maximum tension stress equals

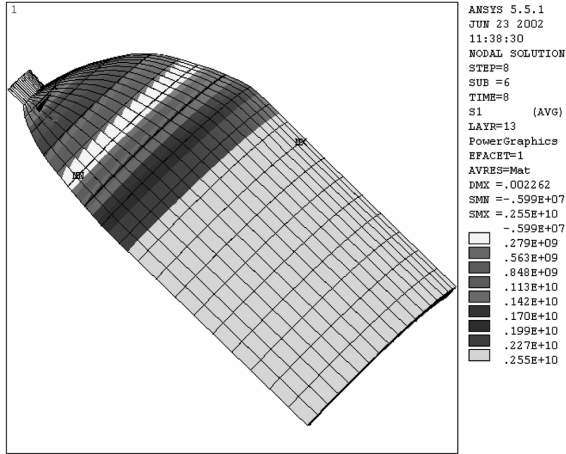


Fig. 6 The distribution of the maximum principal stress (Pa) in FRP vessel under 110 (MPa) internal pressure



Fig. 7 Burst test of FRP vessel under 114 MPa hydrostatic pressure

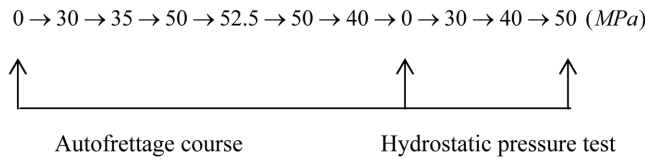


Fig. 8(a) The loading process (Time steps)

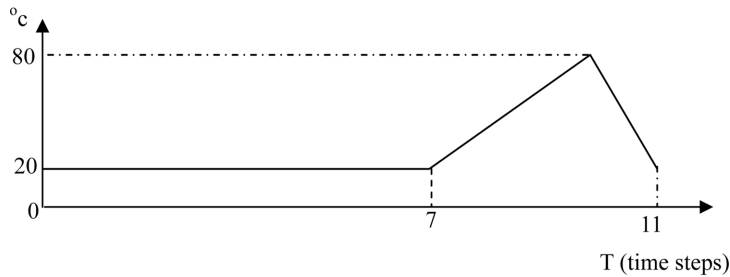


Fig. 8(b) The thermal load (°C) process (Time steps)

the uniaxial tension strength, $\sigma_{Lb} = 2550$ MPa, in the longitudinal direction of fiber, and the distribution of the maximum tension stress in the RFP vessel is shown in Fig. 6. In the really burst test as shown in Fig. 7, the burst pressure is measured to 114 MPa. Comparing the result in Fig. 6 from finite element simulation with the result in Fig. 7 from really burst test, it is seen that the maximum tensile stress in cylindrical part of FRP vessel leads to really burst region appear in the cylindrical part, and both the burst pressure from finite element simulation and the burst pressure measured through burst test is identical, so the above stacking sequence of FRP vessel determined by using finite element simulation satisfies a given burst strength and the requirement of the minimum weight. Thus, an autofrettage process of the FRP vessel with the above stacking sequence is simulated by using a finite element code as follows.

The loading course of autofrettage process for the vessel pressure is divided into 10 steps, which is shown in Figs. 8(a),(b). The loading and unloading course of $0 \rightarrow 52.5 \rightarrow 0$ (MPa) is used to simulate the autofrettage course. After loading, the $0 \rightarrow 50$ MPa is used to simulate the course of hydrostatic pressure experiment. Because the nonlinear computation model is used in the autofrettage course, the step-by-step loading model is applied, which is shown in the Fig. 8(a).

Pressuring process, the temperature in the aluminum liner that directly contacts the gas will increase. The working state of the FRP vessel, under the pressure load and the thermal load after autofrettage, is imitated. The distribution of stress fields in the vessel is calculated. All the calculation parameters are the same as the above, but the load-on pattern is different. The aluminum liner is of thermal elastoplasticity (of Von Mises isotropic hardening mode), the thermal expansion coefficient is $\alpha = 16 \times 10^{-6}/^{\circ}\text{C}$, and the initial temperature of the FRP vessel (reference temperature) is 20°C , when the vessel is loaded to 50 MPa after autofrettage, the temperature will instantly increase to 80°C from 20°C , then the gas pressure remains constant but the temperature decreases gradually to the reference temperature. The thermal load - on process is shown as Fig. 8(b).

During the course of autofrettage, the Von Mises yield Criterion is used for aluminium liner. According to this criterion, when the second stress invariant J_2 is up to one certain value, the material begins to yield, which is

$$\sqrt{J_2} = F(k) \quad (5)$$

The isotropic hardening model is used during the course of calculation, whose characteristics are that the stretching and compressing hardening always take place and develop identically and the yielding surface keep the original shape, expanding and contracting uniformly. The equation of the loading yielding surface is

$$f(\sigma_{ij}) = F(k) \quad (6a)$$

$$k = w_p = \int \sigma_{ij} d\varepsilon_{ij}^p \quad (6b)$$

where the scalar k is one certain measurement of the hardening extent, which can be expressed with plastic work w_p and the $d\varepsilon_{ij}^p$ expresses increment of the plastic strain.

In the finite element simulation of autofrettage process, the Newton iteration method (Iding 1973) is used to solve the nonlinear equation. The allowable value $DTOL$ of the relative displacement of convergence of measurement balance iteration is $1.0E-4$ and the allowable value $FTOL$ of the relative force of convergence of measurement balance iteration is $1.0e-2$. When the relative allowable value of the displacement and force are both reached, the iteration finished. In actual calculation, plastic deformation begins to take place in the aluminium liner when the internal pressure P_s is about 32 MPa. At beginning, when the internal pressure P is up to 30 MPa, the aluminium is still in the elastic deformation stage and the stiffness matrix of the structure stays invariable, which make the computational result is convergent. But under the internal pressure of $30 \text{ MPa} < p < 50 \text{ MPa}$, both the elastic deformation and plastic deformation will take place, so the stiffness matrix K^l will change greatly and it is necessary to decrease the loading step length to guarantee the calculation convergent. Under the biggest internal pressure of 52.5 MPa or so, the loading will be replaced with unloading and the stiffness matrix K^l will also change greatly, so the small loading step length is used at this moment. When the unloading is equal to zero, the

autofrettage course finished. According to the calculation parameters used by finite element simulation of autofrettage, the strain measure to a really FRP vessel is done. The measured FRP vessel is shown in Fig. 9, where strain gauges are adhibited at the measured FRP vessel along the longitudinal direction of the FRP vessel, and are used to the circumferential strain of the FRP vessel. The comparing the result from finite element simulation with the strain measure to a really FRP vessel is shown in Fig. 10, and it is seen the two results are gradually identical as the internal pressure increases. Fig. 13. to Fig. 16 show the distribution of stresses in FRP vessel before and after autofrettage respectively.

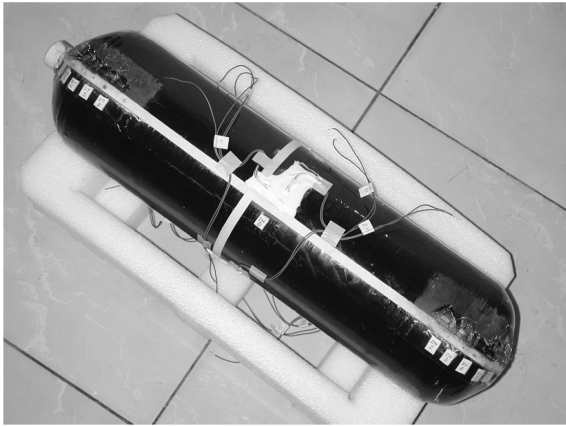


Fig. 9 Strain measure of FRP vessel

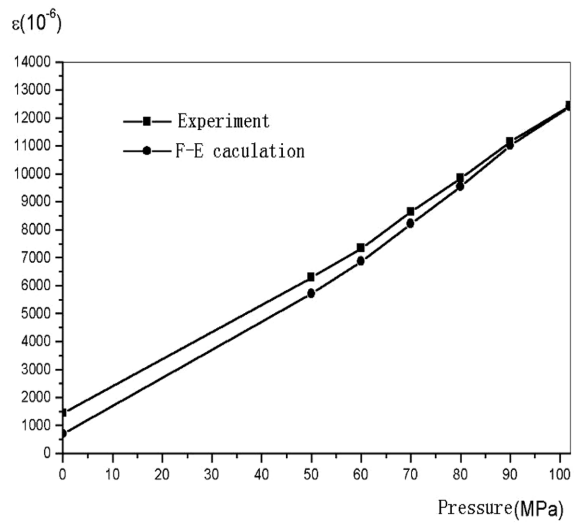


Fig. 10 Strain measure and finite element simulation curves of FRP vessel after autofrettage process

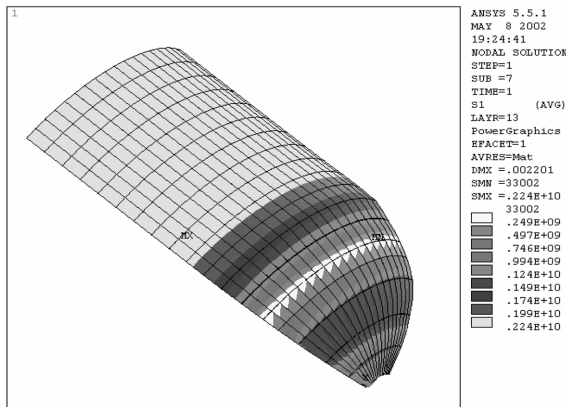


Fig. 11(a) Finite element calculation model of FRP vessel : quarter part with seal end of the FRP vessel

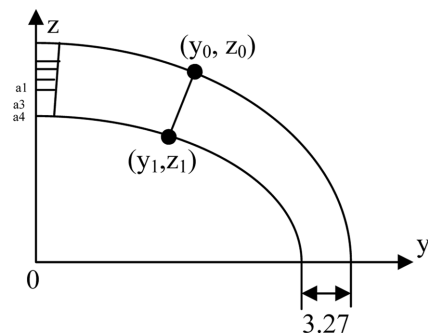


Fig. 11(b) The crackle model of liner seal end with variable thickness

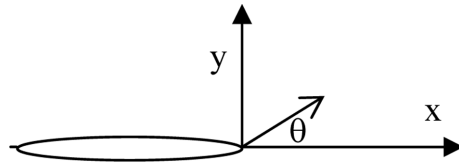


Fig. 12 The coordinate system at crackle

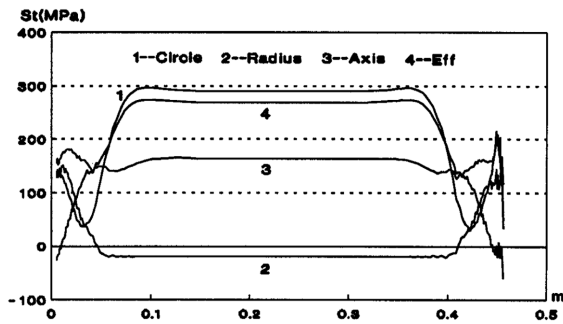


Fig. 13(a) The distribution along Z axis of stress in the liner layer when $p = 30$ MPa before autofrettage

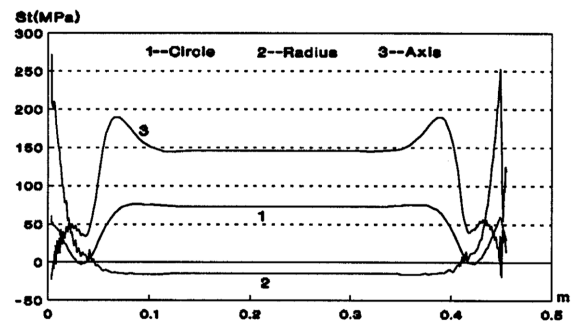


Fig. 13(b) The distribution along Z axis of stress in the helical winding fiber layer when $p = 30$ MPa before autofrettage

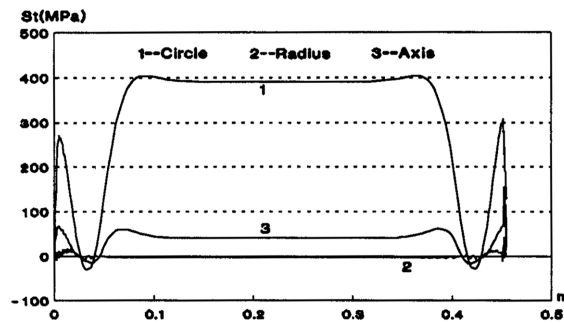


Fig. 13(c) The distribution along Z axis of stress in the circumferential winding fiber layer when $p = 30$ MPa before autofrettage

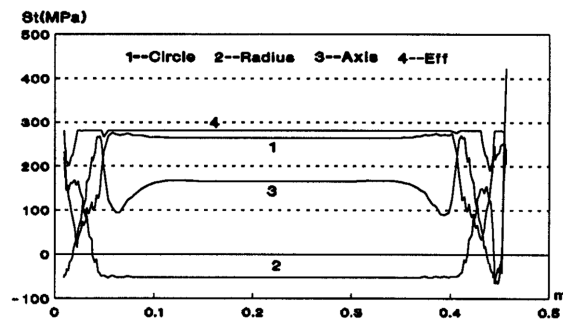


Fig. 14(a) The distribution along Z axis of stress in the liner layer when $p = 52.5$ MPa before autofrettage

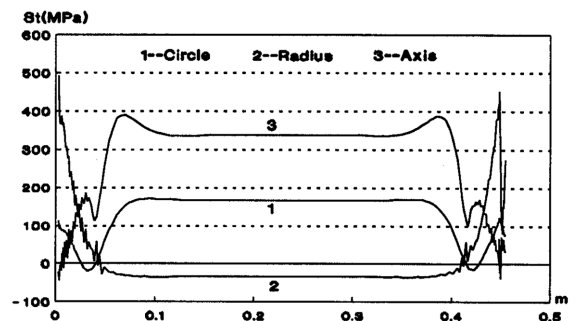


Fig. 14(b) The distribution along Z axis of stress in the helical winding fiber layer when $p = 52.5$ MPa before autofrettage

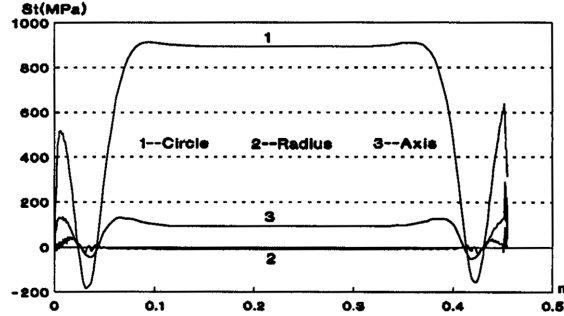


Fig. 14(c) The distribution along Z axis of stress in the circumferential winding fiber layer when $p = 52.5$ MPa before autofrettage

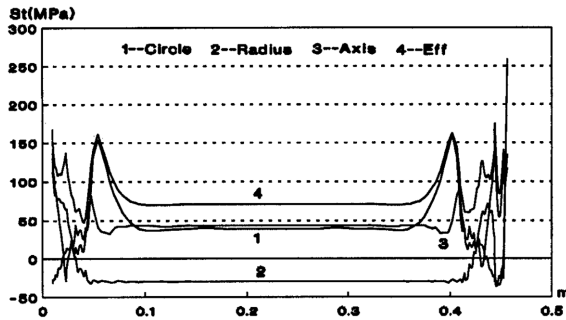


Fig. 15(a) The distribution along Z axis of stress in the liner layer when $p = 30$ MPa after autofrettage

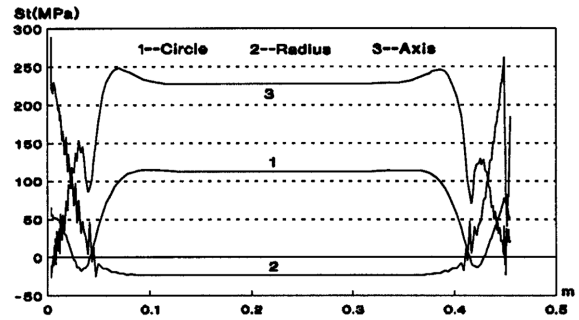


Fig. 15(b) The distribution along Z axis of stress in the helical winding fiber layer when $p = 30$ MPa after autofrettage

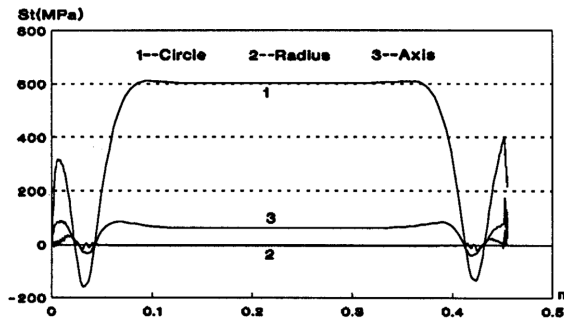


Fig. 15(c) The distribution along Y axis of stress in the circumferential winding fiber layer when $p = 30$ MPa after autofrettage

4. The effect of autofrettage on the crackle on the end of liner

Because of the specificity and complexity of the stress distribution of the top of liner seal end, the flaws and crackles often appear during practical manufacture and application. Here it is presumed that there is a crackle on the top of the aluminium liner seal end. The basic FE model is show in Fig. 11(a), and all the physical parameters stay invariable except that there is only one pin-like

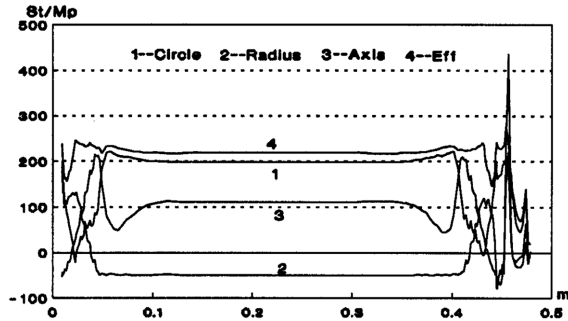


Fig. 16(a) The distribution along Z axis of stress in the liner layer under $p = 50$ MPa and thermal load $\Delta T = 60^\circ\text{C}$ after autofrettage

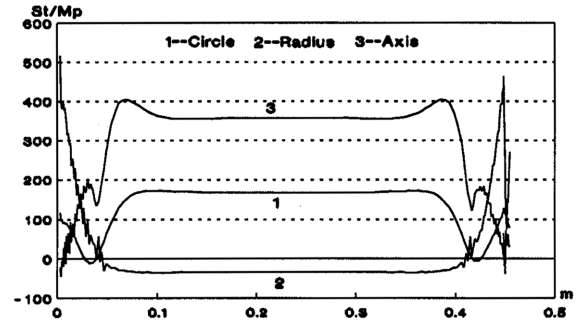


Fig. 16(b) The distribution along Z axis of stress in the helical winding fiber layer under $p = 50$ MPa and thermal load $\Delta T = 60^\circ\text{C}$ after autofrettage

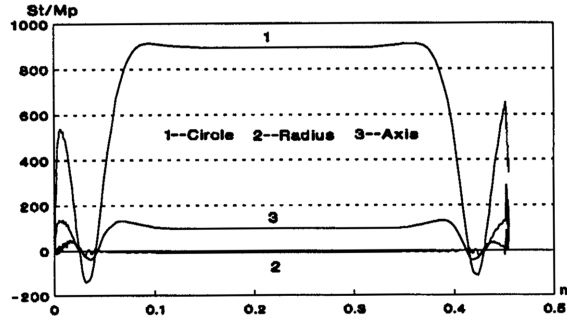


Fig. 16(c) The distribution along Y axis of stress in the circumferential winding fiber layer under $p = 50$ MPa and thermal load $\Delta T = 60^\circ\text{C}$ after autofrettage

crackle. In order to enhance the computational precision, the local grids will be divided more densely, which is shown in Fig. 11(b). The crackle lies from the node $a1$ to node $a4$ and the node $a1$ is the mostly spiry part of the crackle. In this part, a abnormal isoparametric element dividing method is used in the aluminum liner layer, in which the midpoint of the lateral near the crackle point of the 20-node isoparametric element is not located in the normal location but one fourth of the lateral length from the crackle point, which simulates the $r^{-1/2}$ stress singularity at the top of the crackle. The coordinate system is shown in Fig. 12, in which the origin is located at the top of the crackle. When θ equals 0, the expression of the stress field near the top of the crack is

$$\sigma_y = \frac{K_I}{\sqrt{2\pi r}} \left(1 + b_1 \frac{r}{l} + \dots \right) \quad (6)$$

which can also be rewritten as

$$\sqrt{2\pi r} \sigma_y = K_I \left(1 + b_1 \frac{r}{l} + \dots \right) \quad (7)$$

The stress obtained from F-E calculation of every element is σ_y^* and near the crackle point, the stress gradient is a little bigger. When the r/l is very small, stress intensity factor K_I^* can be described by an approximation function which is

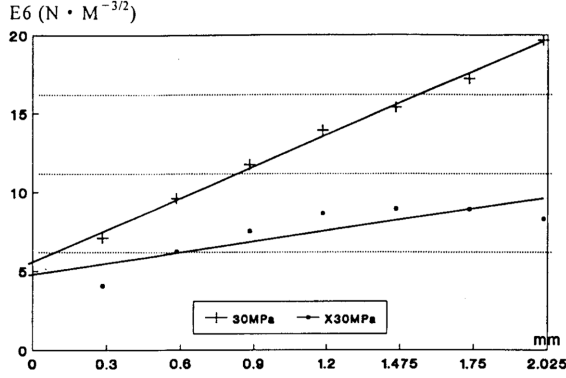


Fig. 17(a) The stress intensity factor of the crack on the metallic liner before and after autofrettage when the structure is under the internal pressure of 30 MPa

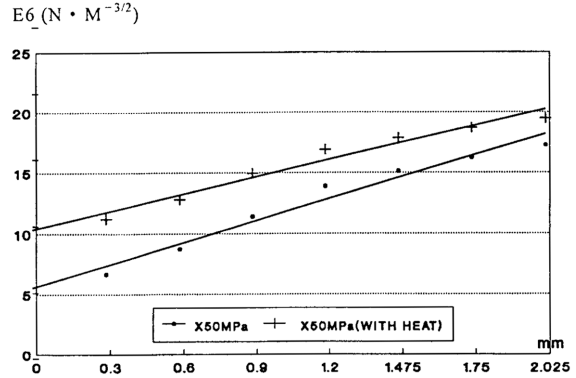


Fig. 17(b) The stress intensity factor of the crack on the metallic liner after autofrettage when the structure is under only the internal pressure of 50 MPa and under the internal pressure 50 MPa with thermal load $\Delta T = 60^\circ\text{C}$

$$K_I^* = \sqrt{2\pi r} \sigma_y^* \tag{8}$$

In the coordinate system with K_I^* as the vertical coordinate and r as abscissa, an extrapolation line is drawn to fit the K_I^* values near the crackle point. When the r equals 0, vertical coordinate of the intersection point of this extrapolation line and vertical axis is the estimation value of the stress intensity factor K_I^* . The calculation result is shown in the Figs. 17(a),(b). Fig. 17(a) shows the extrapolation line of the stress intensity factor of the crackle before and after autofrettage processes when the structure is under the internal pressure of 30 MPa. It can be seen from Fig. 17(a) that the stress intensity factor after autofrettage is smaller than that before autofrettage, which demonstrates that the crackle on the top of the liner seal end has close tendency after the vessel is autofrettage. Fig. 17(b) shows the extrapolation line after autofrettage process when the structure is under only internal pressure of 50 MPa, and the extrapolation line after autofrettage process when the structure is under internal pressure of 50 MPa and thermal load at the same time. The calculation has demonstrated that the stress intensity factor becomes bigger after the thermal load is added, which can explain that the crackle on the top of the liner seal end has opening tendency when the temperature of the liner rises.

5. Discussion

Based on numerical calculations, the ellipse with eccentricity of 0.6 should be chosen as the outer curve of the variable thickness liner seal end to ensure that the aluminium liner is under low stress and that it is manufactured easily. The Ansys F-E program is applied to simulate autofrettage process to a FRP vessel with metallic liner under superpressure, which makes the plastic deformation take place in the aluminium liner while the fiber layer is still under elastic deformation. When the internal pressure is unloaded, the aluminium liner has the original compression stress due to the resilience from the fiber layer while the fiber layer has original stretching stress. Having been

autofrettage, the FRP vessel endures the stress distribution is much more rational.

The analysis of stress fields in FRP vessel before and after autofrettage processes has been shown in Fig. 13 to Fig. 16, and demonstrated that before autofrettage, the stress value in the aluminium liner is very high and reach the yield stress of the liner material when the internal pressure is up to 30 Mpa. While after autofrettage, the stress value in the aluminium liner is very low and only elastic deformation when the vessel is under the same internal pressure. According the Von Mises yield criterion, before autofrettage, the aluminium liner is totally in plastic deformation stage when the internal pressure is up to 50 Mpa. While after autofrettage, the aluminium liner is totally in the elastic deformation stage when the vessel is under the same internal pressure $p = 50$ Mpa. Consequently, the autofrettage process can enhance the bearing capacity, air impermeability and fatigue property of the fiber reinforced pressure vessel with aluminium liner.

The numerical calculations has also been used to demonstrate that autofrettage process can decrease the stress intensity factor of the crackle on the top of the liner end and that, the heat loads can enhance the intensity factor.

6. Conclusions

- 1) The F-E Ansys program may be used to design the optimum structure of fiber reinforced pressure vessel with aluminium liner, and to simulate autofrettage process of the FRP vessel in order to ensure that the vessel has good gas tightness and long fatigue lifetime.
- 2) Some hydrostatic burst experiments and strain measure are used to validate the availability of finite element simulations.
- 3) Through the optimization of the shape of liner ends of fiber reinforced pressure vessel and the simulation of the autofrettage course, the ratio of capacity to weight can reach an perfect value and mean while, it can satisfies the strength requirements under the service internal pressure and thermal load.
- 4) Obviously, the research in this paper has much application value for the actual engineering projects.

References

- Antonelli, V. and Van, T.M. (2001), "Design of composite pressure hull end-closures", *SAMPE J.*, **37**, 15-22.
- Ansys, Inc. ANSYS Analysis Guides Third Edition. SAS, IP Inc., 1997.
- Ben, G., Sakata, K. and Ohta, H. (2006), "Increase of burst pressure and optimum design for CFRP pressure vessels reinforced with SMA wire", *A Hen/Transactions of the Japan Society of Mechanical Engineers, Part A*, **72**, 459-464.
- Iding, R.H. (1973), "Identification of non-line material by finite element method", Report UCSEM 73-4, Dept. Of Civil Engineering, University of California, Berkeley.
- John, W., Tom, Z., Gary, S., Greg, C. and Norman, F. (2004), "Design and testing of large diameter composite reinforced pressure vessels for offshore gas applications", *Proc. of the 23rd Int. Conf. on Offshore Mechanics and Arctic Engineering - Part A: Offshore Technology*, **1**, 235-244.
- Jhung, M.J. and Park, Y.W. (1999), "Deterministic structural and fracture mechanics analyses of reactor pressure vessel for pressurized thermal shock", *Struct. Eng. Mech.*, **8**(1), 103-118.
- Levend, P. and Nuran, K. (2002), "Design of fiber-reinforced composite pressure vessels under various loading conditions", *Compos. Struct.*, **58**, 83-95.

- Liu, J. (1997), "Structural design and analysis of fiber reinforced plastic vessels with load-carrying metallic liner", *Transaction of the Japan Society of Mechanical Engineering, Part A*, **63**, 1758-1765.
- Mirza, S., Bryan, A. and Noori, M. (2001) "Fiber-reinforced composite cylindrical vessel with lugs", *Compos. Struct.*, **53**, 143-151.
- Meng, L.B., Jin, G.C., Yao, X.F. and Yeh, H.Y. (2006), 3D Full-Field Deformation Monitoring of Fiber Composite Pressure Vessel Using 3D Digital Speckle Correlation Method, *Polymer Testing*, **25**(1), 42-48.
- Okamoto, S. and Omura, Y. (2005), "Triaxial stress analysis of cylindrical pressure vessels composed of two layers of orthotropic elasto-plastic materials", *Pressure Vessels Piping Division PVP*, **3**, 41-48.
- Tsai, S.W. and Hahn, H.T. (1980), "Introduction to composite materials", Westport, 1980. CT: Technomic publishing CO.
- Tsai, S.W. (1985), "Composites design", USA, Technomic publishing Think Composites.
- Vasiliev, V.V., Krikanov, A.A. and Razin, A.F. (2003), "New generation of filament-wound composite pressure vessels for commercial applications", *Compos. Struct.*, **62**, 449-459.
- Wild, P.M. and Vichers, G.W. (1997), "Analysis of filament-wound cylindrical shell under combined centrifugal, pressure and axial loading", *Compos. Part A*, **28**, 47-55.
- Xia, M., Kemmochi, K. and Takayanagi, H. (2001), "Analysis of filament wound fiber-reinforced sandwich pipe under combined internal pressure and thermomechanical loading", *Compos. Struct.*, **51**, 273-283.
- Yao, X.F., Xu, W., Xu, M.Q., Jin, G.C. and Yeh, H.Y. (2004a), "Caustic study on stress singularities in laminated composites under concentrated loads", *Int. J. Solid Struct.*, **41**(13), 3383-3393.
- Yao, X.F., Chen, J.D., Jin, G.C., Arakawa, K. and Takahashi, K. (2004b), "Caustic analysis of stress singularities in orthotropic composite materials with mode-I crack", *Compos. Sci. Tech.*, **64**(7-8), 917-924.
- Yao, X.F., Meng, L.B., Guan, J.C. and Yeh, H.Y. (2005), "Full field deformation measurement of fibre composite pressure vessel using digital speckle correlation method", *Polymer Testing*, **24**(2), 245-251.